Parameterization of the Back-Surface Reflection for PERC Solar Cells Including Variation of Back-Contact Coverage

Aina Alapont Sabater, Andreas Fell, Andreas A. Brand, Matthias Müller, and Johannes M. Greulich

Abstract—**Simulation is essential for a comprehensive analysis of the performance of solar cells. The rear contact pitch of passivated emitter and rear cells (PERC cells) is a crucial device parameter that influences not only the electrical performance but also the optical performance of these cells. This article investigates the applicability of the analytical light trapping model by Basore to account for the optical influence of the rear contact pitch as a simpler alternative to ray tracing. First, we manufacture three different groups of cells with different rear contact pitches, where the metallization fraction f_{met} varies between 0 and 54%. Second, the reflectance of the cells is measured. Subsequently, we fit the model parameters R_{f} and R_{b} (internal reflection on the front and back surface, respectively) to the measured reflectance. While we confirm a nonlinear relation between f_{met} and the measurable spectra found in previous works, our results reveal linear relations between f_{met} and R_{b} with the adjusted coefficients of determination of ${R_{\mathrm{adj}}}^2 > 0.97$, as well as between f_{met} and the charge carrier generation rates with ${R_{\mathrm{adj}}}^2 > 0.94$. These relations allow a simple and rapid optical simulation of f_{met} variation for PERC cells. The same approach is likely applicable to any local contacts also in other cell concepts.**

Index Terms—**Light trapping, modeling, optics, photovoltaic cells, reflectance.**

I. Introduction

OPTICAL simulations are an essential part of solar cell research and development. A well-established approach to simulate solar cell optics is detailed 3-D ray tracing, which comes with considerable effort in gathering the simulation inputs, setting the model up, and with significant computation time [1]–[3]. On modern computers and using cloud computing services, the computation times have been reduced a lot over the past 30 years, but still, the computation times are in the range of minutes. Additionally, the user has to select adequate models, e.g., for scattering effects, has to specify the detailed geometries explicitly, and has to specify or select appropriate spectral refractive indices. An alternative approach to 3-D ray tracing consists of using the analytical light-trapping model, as suggested by Basore [4]. It is a widely used optical model in photovoltaics to calculate reflectance, transmittance, and absorptance, as it is implemented in the 1-D device simulator PC1D [5], [6], as well as in the 3-D simulator Quokka3 [7]. This approach is much less computationally expensive and offers computation times significantly below a second, but more model parameters are lumped, i.e., are less physically detailed. If the level of detail is sufficient for the specific simulation task, the simplicity and speed can be a decisive advantage, e.g., when iteratively fitting experimental data.

It has been found that the reflectance, in particular the escape reflectance, depends nonlinearly on the rear metallization fraction in the case of local metallized regions with a lower internal reflection, i.e., on the rear contact pitch [8]. This hindered the application of the Basore and other empirical models such as the Phong model [9] for prediction of the optical generation rate of the passivated emitter and rear cells (PERC cells [10]) with a rear contact pitch variation. In [8], the following linear relation between the spectra of the metallized and contacted (R_{m}) and passivated and uncontacted region (R_{p}) of the back surface was discussed.

$$R\ (\lambda) = f_{\mathrm{met}}\ \cdot R_{\mathrm{m}}\ (\lambda) + (1 - f_{\mathrm{met}}) \cdot R_{\mathrm{p}}\ (\lambda)\,. \qquad (1)$$

Here, f_{met} denotes the metallization fraction of the silicon back surface. It was shown that (1) is not valid [8] and it is, therefore, rejected.

Our goal in this article is to extend and simplify the usage of the Basore model to predict the optical properties of cells with pitch variations.

The rest of this article is organized as follows. In Section II, we describe the manufacturing of the samples and the approach for the optical characterization and simulation. In Section III, we present and discuss the results, finally, Section IV concludes this article.

II. Experimental Details

We manufacture and investigate three groups of samples (group A1, A2, and B, see Fig. 1) in which the rear metallization fraction f_{met} is varied between 0 and 54%. All groups have

Manuscript received February 12, 2021; revised April 13, 2021; accepted May 14, 2021. Date of publication June 4, 2021; date of current version August 20, 2021. This work was supported by the German Federal Ministry for Economic Affairs and Energy within the research project “GENESIS” under Contract 0324274C. *(Corresponding author: Johannes M. Greulich.)*

Aina Alapont Sabater, Andreas Fell, Andreas A. Brand, and Johannes M. Greulich are with the Fraunhofer Institute for Solar Energy Systems, 79110 Freiburg, Germany (e-mail: ainaalapont@gmail.com; andreas.fell@ise.fraunhofer.de; andreas.brand@ise.fraunhofer.de; johannes.greulich@ise.fraunhofer.de).

Matthias Müller is with the Technical University Bergakademie Freiberg, 09599 Freiberg, Germany (e-mail: matth.mueller@physik.tu-freiberg.de).

Color versions of one or more figures in this article are available at https://doi.org/10.1109/JPHOTOV.2021.3082402.

Digital Object Identifier 10.1109/JPHOTOV.2021.3082402

This work is licensed under a Creative Commons Attribution 4.0 License. For more information, see https://creativecommons.org/licenses/by/4.0/

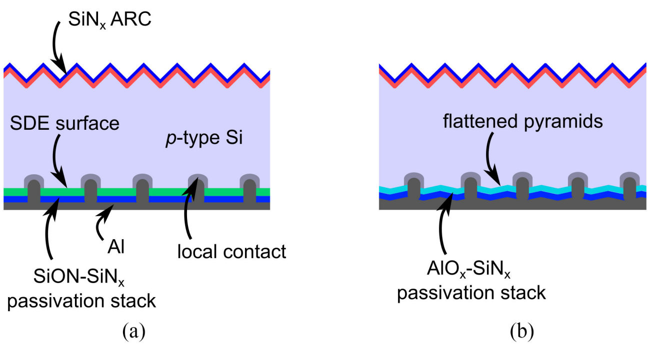

Fig. 1. Schematic cross section of the samples of (a) group A with Centaurus approach and SDE rear surface, and (b) group B with AlO_x approach with flattened pyramids at the rear surface.

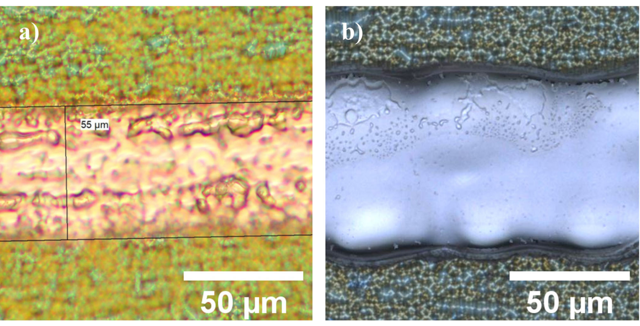

Fig. 3. (a) Exemplary line-shaped LCO of group B. (b) Resulting final contact geometry after aluminum etch back as seen by optical microscopy in top view.

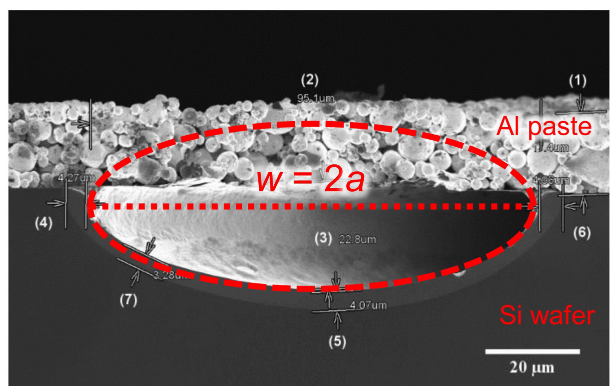

Fig. 2. Example of an SEM measurement of a cross section of a PERC rear contact, with semielliptical cross section and semimajor axis a corresponding to a contact width $w = 2a$. Adapted from [12].

full-area dielectric passivation with line-shaped laser contact openings (LCO). The rear metal is full-area screen-printed aluminum, which forms a local aluminum back-surface field during contact formation in a high-temperature step. The three groups differ in the wafer thickness, the rear side roughness, and the dielectric rear side coatings.

Groups A1 and A2 are two boron-doped Czochralski (Cz) Si wafers (2.2 Ω·cm resistivity, 158 μm thickness after cell process, 156 mm edge length) processed identically according to the Centaurus approach [11] with a textured phosphorous-diffused front side covered with an SiN_x antireflection coating and a saw-damage-edged (SDE) rear side covered with a stack of SiON/SiN_x. Rear side contacting is done by line-patterned laser ablation (LCO) with a pitch variation on every single wafer, the usage of a commercial Al paste for only rear side Al paste screen-printing and standard peak firing in a furnace. The LCO pitch is chosen to 100, 200, 400, 800, 1600 μm, and no ablation. An average contact width is estimated by evaluating scanning electron microscopy (SEM) cross-sectional images. The line contact has a semielliptical cross section, as exemplarily shown in Fig. 2. The semimajor axis a of the ellipse is used to define the contact width $w = 2a$ relevant for optical considerations. With this procedure, a contact width for groups A1 and A2 of 54 μm is determined on parallel processed samples with 1000 μm pitch.

The spectral hemispherical reflectance is measured in 5 nm steps between 300 and 1200 nm using a LOANA system by PVtools GmbH on an area of 20 × 20 mm for each metallization fraction (0%, 3.3%, 6.7%, 13.5%, 27%, 54%). A1 and A2 are basically duplicates of each other, with slight unintended differences in front reflectance. A1 and A2 are intended to show the stability of the sample preparation, measurements, and data analysis.

Group B is also based on boron-doped Cz-Si wafers (1.8 Ω·cm resistivity, 180 μm final thickness, and 156 mm edge length) and then processed according to the AlO_x route, i.e., with KOH textured front side, $POCl_3$ diffused emitter and passivated with an SiN_x antireflection coating, the textured rear side featuring the same textured morphology as the front, slightly planarized by the chemical emitter etch back and then coated with a stack of AlO_x and SiN_x. The LCO geometry is line-shaped with an ablation width of approximately 55 μm ± 4 μm depending on the optical definition of the opening, see Fig. 3(a). In order to maximize the statistical robustness, each wafer contains 25 30 × 30 mm² wide LCO fields in a 5 by 5 array with the different line pitches distributed in a Latin hypercube design [13], preventing a direct correlation of local wafer properties. The line pitches are 247, 386, 540, 690, 1080, 1500, and 2500 μm. There are also fields without LCO. The rear side is then fully coated with a commercial aluminum screen printing paste designed for line-shaped LCO at a thickness of roughly 20 μm. No front-side metallization is applied to the wafers. The firing furnace is set in such a way that the peak wafer temperature reaches 800 °C, which is confirmed via thermocouple measurements. Then, the reflectance spectra are measured between 300 and 1200 nm in 10 nm steps, again with a LOANA system from PVtools GmbH, for each metallization fraction (0%, 3.9%, 6.5%, 7.8%, 9.8%, 13%, 20%, 33%). The wafers are then exposed to an HCl etching solution to etch away the aluminum screen printing. An additional ultrasonic cleaning step removes visible residuals, allowing an unobstructed view of the contact size for optical microscopy, as seen in Fig. 3(b), from which f_{met} is determined for group B.

In order to separate escape reflectance R_{esc} and front external reflectance $R_{\mathrm{f,ext}}$, whose sum is the measured reflectance R, we extrapolate $R_{\mathrm{f,ext}}$ for $\lambda > 950$ nm by fitting a second-degree polynomial to R in the wavelength region 800 nm $< \lambda <$ 950 nm for all reflectance data, as

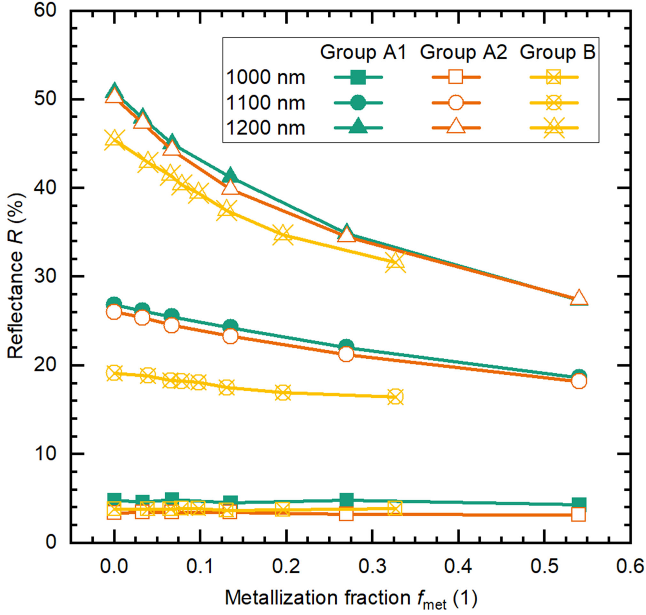

Fig. 4. Measured reflectance R with varying metallization fraction $f_{\rm met}$ of three cell groups, shown here for selected wavelengths (1000, 1100, 1200 nm).

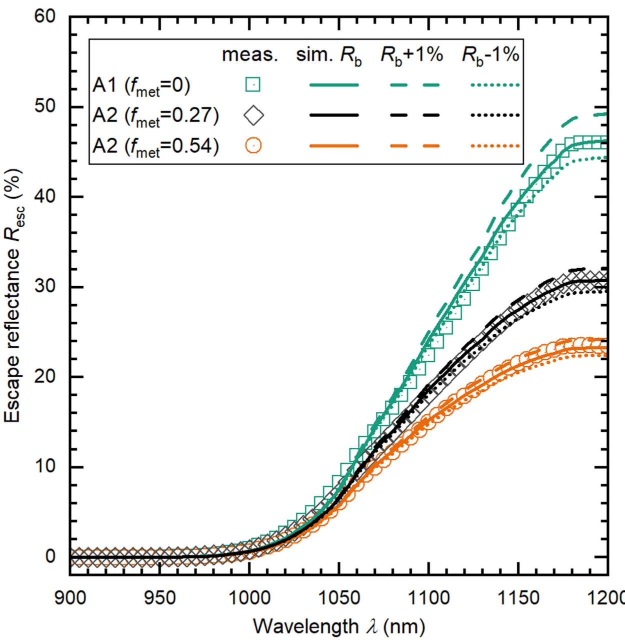

Fig. 5. Simulated and measured escape reflectance $R_{\rm esc}$ for three samples (dashed line: $R_{\rm esc}{}^{\rm sim}$ for $R_{\rm b}+1\%$; dotted line: $R_{\rm esc}{}^{\rm sim}$ for $R_{\rm b}-1\%$).

suggested in [15]. We find using a second-degree polynomial instead of a linear extrapolation to more accurately describe simulated $R_{\rm f,ext}$ spectra.

The optical simulations are performed using the Basore model. As implemented in PC1Dmod, it requires, amongst others, the following six input parameters: internal reflectance on the front surface for first bounce $R_{\rm f1}$ and successive bounces $R_{\rm fn}$, internal reflectance on the back surface for first bounce $R_{\rm b1}$ and successive bounces $R_{\rm bn}$, and type of reflection on the front and back (specular or diffuse). In this article, we use the simplified Basore model explained in [14], where only one reflectance per side is used, i.e., $R_{\rm f1}=R_{\rm fn}=R_{\rm f}$, for the internal reflection at the front side and $R_{\rm b1}=R_{\rm bn}=R_{\rm b}$ for the internal reflection at the back side. Free-carrier absorption (FCA) [16], [17] is not explicitly taken into account and is thereby lumped into the internal reflection parameters. The reader is referred to the literature for the analysis of FCA for solar cells, e.g., [8]. The model parameters are adjusted until the difference between the simulated and measured escape reflectances is minimized in the least square fit using an in-house implementation of the Basore model. Further optical simulations of the reflectance and generation rate are done with PC1Dmod.

TABLE I
FIT AND SIMULATION RESULTS OF THE SIMPLIFIED BASORE MODEL

Group	$f_{\rm met}$ (1)	$R_{\rm f}$ (%)	$R_{\rm b}$ (%)	$j_{\rm ph}$ (mA/cm^2)
A1	0	88	89	41.31
A1	0.033	88	87	41.18
A1	0.067	88	86	41.13
A1	0.135	88	84	41.02
A1	0.27	88	80	40.81
A1	0.54	88	72	40.45
A2	0	88	89	41.52
A2	0.033	88	88	41.47
A2	0.067	88	86	41.34
A2	0.135	88	83	41.18
A2	0.27	88	80	41.02
A2	0.54	88	73	40.70
B	0	93	92	41.90
B	0.0392	93	91	41.84
B	0.06533	93	90	41.76
B	0.0784	93	90	41.76
B	0.098	93	89	41.70
B	0.13067	93	88	41.62
B	0.196	93	87	41.55
B	0.32667	93	85	41.42

III. RESULTS AND DISCUSSION

Fig. 4 shows the relation between measured reflectance and metallization fraction for selected wavelengths, especially in the long-wavelength region ($\lambda > 1100$ nm), which confirms the nonlinearity of the reflectance and the invalidity of (1), as also found in [8].

Using the escape reflectance determined from the measured reflectance spectra as an input parameter in our simulation program, we determine the fit parameters $R_{\rm f}$ and $R_{\rm b}$. Fig. 5 exemplarily shows three measured escape spectra and the corresponding fit. An excellent agreement is found. A constant value of $R_{\rm f}$ for all the cells within a group is obtained, i.e., 88% for groups A1 and A2, and 93% for group B (see Table I). This confirms the consistency of the measurement data and the applicability of the simplified Basore model.

It must be noted that in PC1Dmod, the parameters $R_{\rm f}$ and $R_{\rm b}$ can be varied in steps of 1%. In order to check the accuracy and to see the effect of this difference on the escape reflectance as

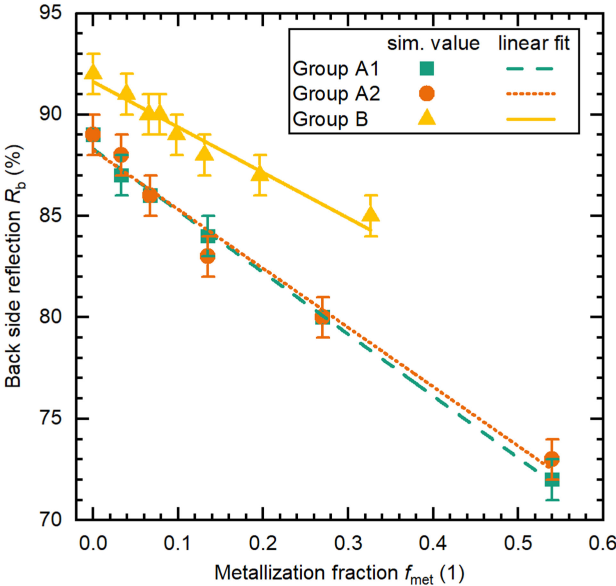

Fig. 6. Back-side reflectance R_{b} with varying metallization fraction f_{met} of three cell groups.

TABLE II
RESULTS OF THE LINEAR FITS OF (2)

Group	R_{pass} (%)	*Std. err.* (R_{pass}) (%)	R_{met} (%)	*Std. err.* (R_{met}) (%)	R_{adj}^2
A1- R_b	88.30	0.24	57.85	0.78	0.995
A2- R_b	88.25	0.51	59.1	1.7	0.977
B- R_b	91.62	0.28	69.2	1.6	1.000

The standard errors are calculated from the square root of the diagonal elements of the covariance matrix multiplied with the mean residual variance.

TABLE III
RESULTS OF THE LINEAR FITS OF (3)

Group	j_{pass} (mA/m²)	*Std. err.* (j_{pass}) (mA/cm²)	j_{met} (mA/cm²)	*Std. err.* (j_{met}) (mA/cm²)	R_{adj}^2
A1- j_{ph}	41.252	0.021	39.721	0.070	0.986
A2- j_{ph}	41.466	0.036	39.98	0.12	0.957
B- j_{ph}	41.867	0.021	40.38	0.12	0.941

well as on the charge carrier generation rate, here expressed as photogenerated current density j_{ph}, we perform a small variation of R_{b} in our simulations. The results, depicted in Fig. 5, show the simulated escape reflectance R_{esc} for the three scenarios of R_{b} (best fit R_{b}, $R_{\mathrm{b}} + 1\%$, and $R_{\mathrm{b}} - 1\%$) for each of the three samples. As can be seen, the variation of R_{b} by $1\%_{\mathrm{abs}}$ induces a noticeable change in the reflectance, in particular for smaller metallization fractions $f_{\mathrm{met}} < 20\%$, which is the relevant range for typical PERC cells. This means that a 1% error of the fit parameters can be considered as an upper bound for the R_{b} uncertainty. For the same model parameters, we calculate j_{ph}. When R_{b} is varied by $\pm 1\%_{\mathrm{abs}}$, j_{ph} is changed by up to ± 0.08 mA/cm^2, i.e., $\pm 0.19\%_{\mathrm{rel}}$. These values are upper bounds of the uncertainty of the j_{ph} simulation. We consider the values negligible for a f_{met} optimization, and thus, judge the simulations to be sufficiently accurate for $f_{\mathrm{met}} < 20\%$.

Although the external reflectance does not depend linearly on the metallization fraction, the simulations using the Basore model yield a linear relation

$$R_{\mathrm{b}} = (1 - f_{\mathrm{met}}) \cdot R_{\mathrm{pass}} + f_{\mathrm{met}} \cdot R_{\mathrm{met}} \quad (2)$$

between the internal reflectance R_{b} and the metallization fraction f_{met}, as can be seen in Fig. 6. The fit parameters R_{pass} and R_{met} correspond to the internal reflection parameters in the passivated and metallized regions, respectively. The adjusted coefficient of determination $R_{\mathrm{adj}}{}^2$ varies between 0.977 and 1.000 (see Table II), evidencing a highly linear relation. For groups A1 and A2, the fit parameters are the same, within the standard errors. This is expected since A1 and A2 are processed identically, further increasing the confidence in the results.

The R_{b} at $f_{\mathrm{met}} = 0$, i.e., the internal reflection coefficients for the passivated areas R_{pass}, differ between A1 and A2 ($\sim$88.3%) and group B (91.62%). We attribute this to differences of the two rear-side properties (surface morphology, passivation layers, Al paste properties) and different amounts of FCA that are lumped with the internal reflectance parameters.

Also, the extrapolated R_{b} at $f_{\mathrm{met}} = 1$, i.e., the reflection coefficients for the metallized areas R_{met}, differ between A1 and A2 ($\sim$58%) and group B ($\sim$69%). We speculate that this difference might be induced primarily by different rear surface roughness and different optical properties of the Al back-surface field and the eutectic layer and different amounts of void formation [18] of the two datasets and, hence, might have a physical origin in the silicon rear surface preparation, the Al pastes, and/or firing conditions, which were different for groups A and B. Comparable differences of the resulting reflection spectra are also apparent from the literature, e.g., comparing Fig. 4 in [19] and Fig. 3 in [20]. We judge possible differences of the methods for measuring the metallization fraction to have only a small impact on R_{met}: For explaining the full difference, an error of the f_{met} determination of $30\%_{\mathrm{rel}}$ to $40\%_{\mathrm{rel}}$ for groups A1 and A2 would have occurred. However, we expect a maximum error of $10\%_{\mathrm{rel}}$ and hence can attribute only up to a third or a fourth part of the R_{met} difference to an error in determining f_{met}.

Similar to (2), a linear relationship

$$j_{\mathrm{ph}} = (1 - f_{\mathrm{met}}) \cdot j_{\mathrm{pass}} + f_{\mathrm{met}} \cdot j_{\mathrm{met}}. \quad (3)$$

between the photogenerated current density j_{ph} and metallization fraction f_{met} can be established with adjusted coefficients of determination $R_{\mathrm{adj}}{}^2$ between 0.941 and 0.989, as shown in Fig. 7 and detailed in Table III. The fit parameters j_{pass} and j_{met} correspond to the photogeneration in the passivated and metallized regions, respectively. However, the $R_{\mathrm{adj}}{}^2$ is somewhat lower compared with R_{b}, indicating that the area-averaging of R_{b} provides a physically more accurate representation of the cell optics. Keep in mind that we round the values of R_{b} with a precision of $1\%_{\mathrm{abs}}$.

As an addition to j_{ph} determined with the values according to Table I (best fit of escape reflectance) and the linear fit of $j_{\mathrm{ph}}(f_{\mathrm{met}})$ according to (3), we added the j_{ph} as simulated with the values of R_{b} according to (2) and Table II. These data show a slight nonlinearity, which is visible in Fig. 7. Such a nonlinearity

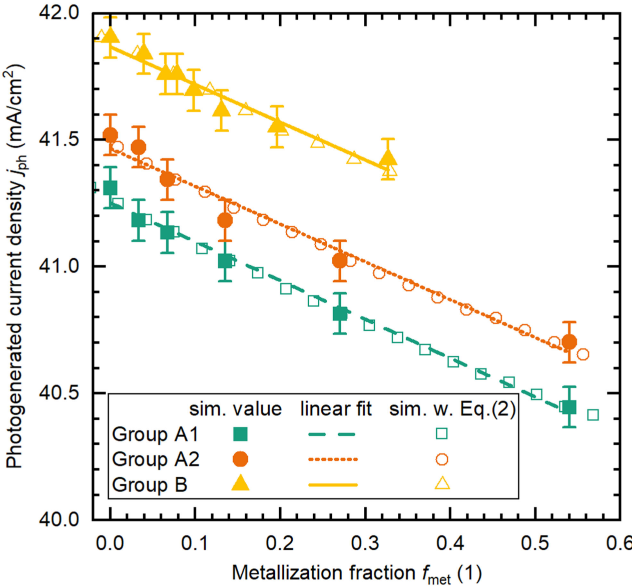

Fig. 7. Photogenerated current density j_{ph} with varying metallization fraction f_{met} of three cell groups.

is expected due to the fact that a part of the light is internally reflected not only once, but several times before being absorbed, in particular in the case of a highly reflective back surface. On an absolute level, the deviations of the values from the linear fit are below 0.1 mA/cm², which we judge acceptable for many applications.

IV. Conclusion

Our investigations using the analytical light trapping model by Basore revealed a linear relationship between the rear metallization fraction f_{met} and the internal reflectance on the back side R_{b}, as well as with the photogenerated current density j_{ph} of PERC cells with adjusted coefficients of determination $R_{\mathrm{adj}}{}^2$ above 0.97 and 0.94, respectively. The reflectance spectra of only two samples with significantly different rear contact fractions are required to determine R_{met} and R_{pass} by fitting the Basore model and, hence, to determine the linear relation for the specific device properties. Alternatively, the data given in the present work can be applied to partly or fully replace the experiments for the determination of R_{met} and R_{pass}. The linearity, thus, enables the application of the Basore model to describe the influence of varying rear contact fraction, providing a simpler and rapid optical modeling alternative to ray tracing for this task.

Because of the optical equivalency of the local rear contacts of PERC cells investigated in this work with other local contacts, we expect the area-averaging of the reflection coefficients to be valid also, e.g., at the front side of PERC, TOPCon or silicon heterojunction solar cells, and at the rear side of back-contact back-junction solar cells.

References

[1] N. Wöhrle, J. Greulich, C. Schwab, M. Glatthaar, and S. Rein, “A predictive optical simulation model for the rear-surface roughness of passivated silicon solar cells,” *IEEE J. Photovolt.*, vol. 3, no. 1, pp. 175–182, Jan. 2013.

[2] S. Baker-Finch and K. R. McIntosh, “One-dimensional photogeneration profiles in silicon solar cells with pyramidal texture,” *Prog. Photovolt., Res. Appl.*, vol. 20, no. 1, pp. 51–61, 2012.

[3] P. Campbell and M. A. Green, “Light trapping properties of pyramidally textured surfaces,” *J. Appl. Phys.*, vol. 62, no. 1, pp. 243–249, 1987.

[4] P. A. Basore, “Extended spectral analysis of internal quantum efficiency,” in *Proc. 23rd IEEE Photovolt. Spec. Conf. Louisville*, Louisville, KY, USA, 1993, pp. 147–152.

[5] H. Haug and J. Greulich, “PC1Dmod 6.2—Improved simulation of c-Si devices with updates on device physics and user interface,” *Energy Procedia*, vol. 92, pp. 60–68, 2016.

[6] D. A. Clugston and P. A. Basore, “PC1D version 5: 32-bit solar cell modeling on personal computers,” in *Proc. 26th IEEE Photovolt. Spec. Conf. Anaheim*, Anaheim, CA, USA, 1997, pp. 207–210.

[7] A. Fell, J. Schön, M. C. Schubert, and S. W. Glunz, “The concept of skins for silicon solar cell modeling,” *Sol. Energy Mater. Sol. Cells*, vol. 173, pp. 128–133, 2017.

[8] D. Kray, M. Hermle, and S. W. Glunz, “Theory and experiments on the back side reflectance of silicon wafer solar cells,” *Prog. Photovolt., Res. Appl.*, vol. 16, no. 1, pp. 1–15, 2008.

[9] B. T. Phong, “Illumination for computer generated pictures,” *Commun. ACM*, vol. 18, no. 6, pp. 311–317, 1975.

[10] A. W. Blakers, A. Wang, A. M. Milne, J. Zhao, and M. A. Green, “22.8% efficient silicon solar cell,” *Appl. Phys. Lett.*, vol. 55, no. 13, pp. 1363–1365, 1989.

[11] K. A. Münzer *et al.*, “Technical performance and industrial implementation in favour of centaurus technology,” *Energy Procedia*, vol. 27, pp. 631–637, 2012.

[12] M. Müller *et al.*, “Impact of local back-surface-field thickness on open-circuit voltage in PERC solar cells: An experimental study applying ANOVA to determine critical sample size necessary to differentiate mean LBSF values with statistical significance,” *IEEE J. Photovolt.*, vol. 10, no. 6, pp. 1642–1647, Nov. 2020.

[13] M. D. McKay, R. J. Beckman, and W. J. Conover, “A comparison of three methods for selecting values of input variables in the analysis of output from a computer code,” *Technometrics*, vol. 21, no. 2, 1979, Art. no. 239.

[14] A. Fell, W. Wirtz, H. Höffler, and J. Greulich, “Determining the generation rate of silicon solar cells from reflection and transmission measurements by fitting an analytical optical model,” in *Proc. 46th IEEE Photovolt. Spec. Conf. Chicago*, Chicago, IL, USA, 2019, pp. 3037–3041.

[15] R. Brendel *et al.*, “Breakdown of the efficiency gap to 29% based on experimental input data and modeling,” *Prog. Photovolt., Res. Appl.*, vol. 24, no. 12, pp. 1475–1486, 2016.

[16] M. Rüdiger, J. Greulich, A. Richter, and M. Hermle, “Parameterization of free carrier absorption in highly doped silicon for solar cells,” *IEEE Trans. Electron Devices*, vol. 60, no. 7, pp. 2156–2163, Jul. 2013.

[17] S. C. Baker-Finch, K. R. McIntosh, D. Yan, K. C. Fong, and T. C. Kho, “Near-infrared free carrier absorption in heavily doped silicon,” *J. Appl. Phys.*, vol. 116, no. 6, 2014, Art. no. 63106.

[18] E. Urrejola, K. Peter, H. Plagwitz, and G. Schubert, “Silicon diffusion in aluminum for rear passivated solar cells,” *Appl. Phys. Lett.*, vol. 98, no. 15, 2011, Art. no. 153508.

[19] E. Urrejola *et al.*, “High efficiency industrial PERC solar cells with all PECVD-based rear surface passivation,” in *Proc. 26th Eur. Photovolt. Solar Energy Conf. Exhib.*, Hamburg, Germany, 2011, pp. 2233–2235.

[20] J. Müller, S. Gatz, K. Bothe, and R. Brendel, “Optimizing the geometry of local aluminum-alloyed contacts to fully screen-printed silicon solar cells,” in *Proc. 38th IEEE Photovolt. Spec. Conf. Austin*, Austin, TX, USA, 2012, pp. 2223–2228.